Astron. Astrophys. 356, 840–848 (2000)

ASTRONOMY AND ASTROPHYSICS

QSO mass constraints from gravitational lensing studies of quasar pairs

The cases of Q1548+114 A & B and Q1148+0055 A & B⋆

J.-F. Claeskens⋆⋆, Dong Wook Lee, M. Remy, D. Sluse, and J. Surdej⋆⋆⋆

Université de Liège, Institut d'Astrophysique et de Géophysique, Avenue de Cointe 5, 4000 Liège, Belgium

Received 17 January 2000 / Accepted 17 February 2000

Abstract. New constraints on the mass of quasars are derived from gravitational lensing studies of the QSO pairs Q1548+114 A & B and Q1148+0055 A & B, for which new ground-based and Hubble Space Telescope (HST) direct imagery have been obtained. In the case of Q1548+114 A & B, QSO A has been resolved into its host galaxy and a close companion. The non-detection with HST of a secondary lensed image of the background QSO in the close vicinity of the foreground one and the modeling of the host of QSO A, of the companion and of field galaxies with Singular Isothermal Spheres (SIS) yield a robust upper limit on the central compact mass of $4.5\,10^{11}\mathrm{M}_{\odot}$. On the other hand, the combined mass of Q1148+0055 B plus host must be smaller than $6.5\,10^{11}\mathrm{M}_{\odot}$ since no secondary lensed image has been detected with HST. Photometry and relative astrometry of all the detected objects are reported.

Key words: cosmology: gravitational lensing – galaxies: quasars: general – galaxies: quasars: individual: Q1548+114 A&B – galaxies: quasars: individual: Q1148+005 A&B

1. Introduction

While the accretion disk surrounding a massive black hole (MBH) is the current paradigm to explain the huge amount of energy radiated by Active Galactic Nuclei (AGN; see e.g. Krolik 1999), observational evidence and constraints on the mass of MBHs in AGNs are difficult to set. The glare of the AGN itself prevents the direct observation of the stellar kinematics close to the central part. This can only be done for nearby normal galaxies, where a correlation between the mass of the central black hole and that of the bulge has been found (Magorrian et al. 1998). For distant quasars, a rough estimate of the mass of the MBH relies on the size and velocity dispersions of the broad-line region (e.g. Padovani & Rafanelli 1988) and is affected by systematics. Gravitational lensing studies may provide an independent estimate of the quasar mass through its effects on our view of background objects. Close pairs of quasars with angular separations of a few arcseconds on the sky and with different redshifts are suitable to determine (constrain) the mass of the foreground one from the (non)detection of a secondary lensed image of the distant one.

Such a pair of quasars (Q1548+114 A & B; $z_A = 0.44$, $z_B = 1.90$, $\Delta\theta = 4.9''$) has been first discovered by Wampler et al. (1973). Gott & Gunn (1974) argued that gravitational lensing effects due to the foreground quasar on light from the background one should appreciably enhance the chance of observing such a tight pair of quasars; this effect being referred to-day as the amplification – or magnification – bias. They also showed that the absence of a secondary lensed image of B near the foreground quasar requires the combined mass of A and of its host galaxy to be less than $7\,10^{12}M_{\odot}$. Let us note that a close group of three galaxies has been found at approximately $10''$ West of quasar A and at nearly the same redshift (Stockton 1974). Shaver & Robertson (1985) obtained an R-band CCD image of this quasar pair under average seeing conditions and made a search for the presence of a secondary image of QSO B near quasar A. No such a secondary image, with an intensity greater than 1 percent that of B and further away than $1''$ from quasar A, could be detected. Iovino & Shaver (1986) used these observations to refine the upper limit on the mass of the foreground quasar. They found that the mass of quasar A is less than $2\,10^{12}M_{\odot}$ and they derived an upper limit of 0.3 g/cm^2 for the surface mass density of any associated cluster.

We have proposed to use the WFPC2 planetary camera onboard the Hubble Space Telescope (HST) in order to set more stringent observational constraints on the presence of a secondary image, i.e. setting a larger magnitude difference between the primary and secondary QSO images at smaller angular separations, for this and two more recently reported pairs of quasars (Q1148+0055 A & B and Q1009-0252 A, B & C) having different redshifts and angular separations smaller than $5''$ (Surdej et al. 1993; Hewett et al. 1994)[1]. The case of Q1009-0252 A-C,

Send offprint requests to: claesken@astro.ulg.ac.be

⋆ Based on data collected with the Hubble Space Telescope and at the European Southern Observatory, La Silla, Chile

⋆⋆ Chargé de recherches du F.N.R.S. (Belgium)

⋆⋆⋆ Directeur de recherches du F.N.R.S. (Belgium)

[1] The detection of two quasar pairs alike Q1009-252 and Q1148+0055 in the LBQS is *not* unlikely (Hewett et al. 1998).

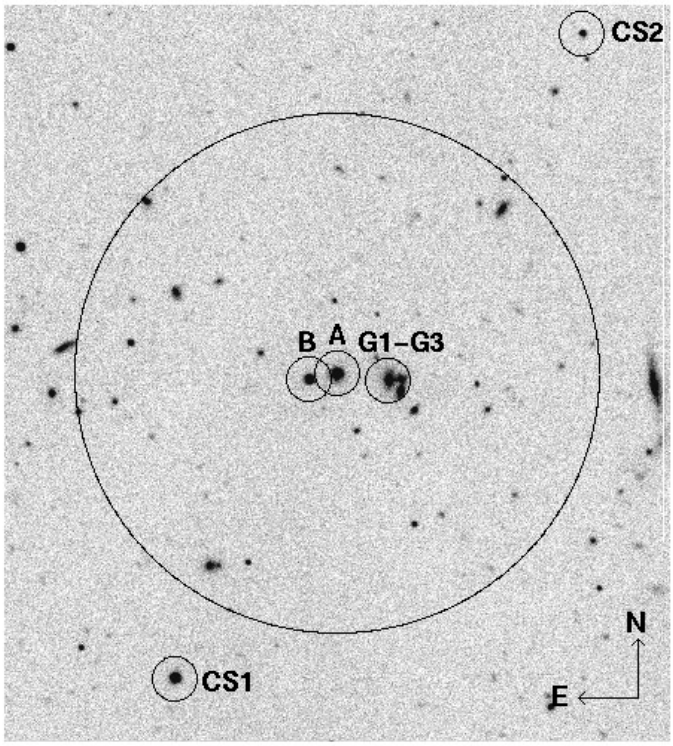

Fig. 1. Field centered on Q1548+114 A from the coadded ground-based R band observations. The large $45''$ radius circle represents the region where field galaxy photometry has been performed using SExtractor. Small circles identify the quasars A & B, the comparison stars CS1 & CS2 and the 3 bright galaxies G1-G3 about $10''$ West of QSO A.

consisting of two lensed QSO images A & B and a foreground quasar C located at a distance of $4.6''$, will be reported in another paper (Surdej et al. 2000). In Sects. 2-3, we report on HST observations for Q1548+114 A & B together with complementary ground-based observations. In Sect. 4, we present the lensing model and in Sect. 5 we discuss the results. The observations of Q1148+0055 A & B are reviewed in Sect. 6. Conclusions form the last section. Cosmological parameters are fixed to $\Omega_0 = 1$, $\lambda_0 = 0$ and $H_0 = 65$ km/s/Mpc.

2. Observations of Q1548+114 A & B

2.1. Ground-based observations

Q1548+114 A & B has been imaged at the European Southern Observatory (E.S.O., La Silla, Chile) under very good seeing conditions, with the SUSI direct camera mounted at the Nasmyth focus of the New Technology Telescope (NTT) during test time on $10^{\rm th}$ of May 1994. The Tektronix CCD # 25 was used. The scale is $0.128''$/pixel. Three exposures of 3min were obtained in the R band, with an average seeing of $0.64''$. These frames have been reduced following the standard procedure but flux calibration is missing. A scaled Point Spread Function (PSF) subtraction analysis (see Sect. 3.2) reveals a fuzzy source close to component A. This reinforced our decision to apply for observing time with HST.

In addition, we retrieved a set of 8 images of Q1548+114 observed in the R band with the E.S.O./M.P.I. 2.2m telescope + direct CCD camera in sub-arcsecond seeing conditions; the image scale is $0.175''$/pixel. The frames were obtained during the March 1993 observations related to the *Gravitational Lensing* Key-Program, together with standard stars to allow photometric calibrations. The total exposure time amounts to 40min. After precise alignment and scaling, these frames were coadded together with the NTT frames in order to create the deepest image of the $\simeq 1$ arcmin field around Q1548+114 A & B (see Fig. 1).

2.2. HST observations

Our HST observations of Q1548+114 A & B consist of 4 frames acquired with the WFPC2 planetary camera (PC1; scale: $0.0455''$/pixel) through the F814W wideband filter (PID: 6790, PI: J. Surdej) on February 12, 1999. In order to avoid saturation of the bright pointlike image of component A, we chose an integration time of 400 sec and a gain of 15 e/ADU. Unfortunately, the last image cannot be used for PSF analysis because of the huge number of cosmic hits, some affecting the QSO images.

Q1548+114 A & B have also been observed in May 1995 with the Wide Field camera through the F702W filter (PID: 5682, PI: M. Burbidge) with an exposure time of 700 sec. Although the central parts of QSO A and QSO B are saturated, these data provide useful information on the close vicinity of QSO A.

3. Analysis of the observations of Q1548+114 A & B

3.1. Aperture photometry

Aperture photometry in the R band of Q1548+114 A & B and of the two comparison stars CS1 & CS2 (see Fig. 1) has been derived from the flux calibrated ground-based observations obtained on $20^{\rm th}$ of March 1993, using Johnson-Kron-Cousins standard stars (Landolt 1992) and the value of the extinction coefficient $k_R = 0.067$ available on the WEB for that night (Burki et al. 1995). The magnitude difference between the two comparison stars being unchanged on the uncalibrated NTT observations, we made use of those stars to perform a secondary flux calibration of the NTT frames. The results are reported in Table 1.

While the Q1548+114 B flux remained constant within the error bar, our observations show that component A has dimmed by 0.15 mag between March 1993 and May 1994. The smallest magnitude difference observed in R between components A & B is thus about 0.22 mag while it was between 0.7 and 0.9 mag in 1983 (Shaver & Robertson 1985; Yee et al. 1986). The optical variability of Q1548+114 A is not surprising as its core is a known variable radio-source (Barthel et al. 1984).

The HST aperture magnitudes listed in Table 1 rely on the PHOTFLAM keyword and they have been derived according to the standard procedure described in Whitmore (1997). A CTE correction of 0.02 mag has been performed and the F814W magnitudes have been offset to the Vega system (I_C Kron-Cousins magnitudes; no colour term was added).

Table 1. Aperture photometry of Q1548+114 A+host & B. The estimated error bar is 0.05 mag.

Date	Telescope	Filter	Component A	Component B	CS1	CS2
20 March 1993	2.2m ESO/MPI	R	18.42	18.82	18.40	20.73
10 May 1994	NTT	R	18.57	18.79	18.40	20.73
12 February 1999	HST	I_c	17.55	18.23	-	-

Finally, since light may be considered as a tracer of mass, we measured with SExtractor (Bertin & Arnouts 1996) the apparent R magnitude of all field galaxies detected within $45''$ of QSO A on the deep coadded ground-based image, including the three bright galaxies G1-G3 seen in Fig. 1. The detection criterion corresponds to a limiting magnitude $m_{R,lim}$ of 24 mag/arcsec^2, significantly deeper than the HST direct imagery.

3.2. PSF analysis

Q1548+114 A directly appears to be a diffuse object on both the NTT and HST frames. A careful subtraction of a pointlike component corresponding to the QSO itself is required in order to better quantify the nature of the underlying extended object (e.g. the host galaxy). This is done by fitting simultaneously the intensity and position of the numerical PSF to the QSO contribution with an analytical model for the extended component. We used the program developed by Remy (1997). We first present the results from the ground-based observations, then from the archive images and finally from our own HST frames.

On each NTT frame, the numerical PSF has been estimated from QSO B and the two stars CS1 and CS2. Simultaneous fits of the PSF together with either a gaussian, exponential or de Vaucouleurs model for the diffuse component have been performed. The results are equivalently good in terms of the reduced χ^2, which is of the order of unity, or residuals, which are all compatible with the statistical noise in the original images. The magnitude of the pointlike component is given by the integrated count number in the PSF while the magnitude of the galaxy has been estimated using SExtractor in the same way as for the field galaxies but after subtracting a scaled PSF from the original image. The magnitude estimates are very similar for the different models. They are reported in the first part of Table 2 together with the fitted positions.

The center position of the diffuse object is significantly offset with respect to that of the QSO on the ground-based images (Table 2). The HST archive images indicate that this is due to a companion galaxy located at about $1.1''$ (~ 5 kpc) from the QSO and about 2 mag fainter than the host. Indeed, a synthetic PSF has been generated with the `TINYTIM` software package (Krist & Hook 1996) from the unsaturated pixels of QSO B and a scaled PSF subtraction has been performed on QSO A after giving a zero weight to the central saturated pixels. Considering only QSO A and a single extended object, their relative positions are found in agreement with those obtained from the ground-based observations, but residuals are present. Adding a second gaussian component considerably improves the fit; its position is found to coincide with that of the previous residuals, while the first component is then centered on the QSO to better than half a pixel and thus corresponds to the host galaxy (see Fig. 2). Because of saturation, aperture photometry has only been performed for the companion, following Holtzmann et al. (1995). Assuming $z \sim 0.5$, we chose a color term $V - R \sim 1$ (Fukugita et al. 1995). The photometry and the relative positions are listed in the central part of Table 2.

The presence of closeby companions in the vicinity of QSOs, especially when the host is an elliptical galaxy, has already been evidenced by Bahcall et al. (1997) and seems to be connected to the AGN process and to the QSO environment. In the case of Q1548+114 A, an extended emission line region has already been reported by Stockton & MacKenty in 1987. The host appears to be a typical L_* galaxy. The image is not deep

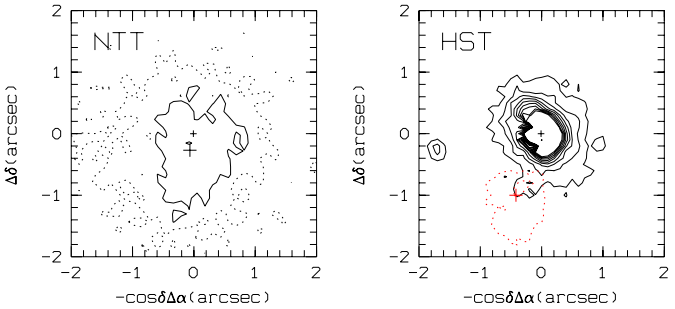

Fig. 2. Contour plots of the underlying objects in the R band after scaled PSF subtraction of Q1548+114 A. The external contours are at the 3σ level. Left: from ground-based images; the small (resp. large) cross indicates the QSO A (resp. host) position. Right: from HST archive image; the small (resp. large) cross indicates the QSO A + host (resp. companion) position; full lines define the host while dotted contours delineate the companion.

Table 2. PSF analysis of Q1548+114 A. The error bars reflect the dispersion of the results using different models and the error on the zero point for the NTT magnitudes.

NTT	$\Delta\alpha\cos\delta('')$	$\Delta\delta('')$	R
QSO A	$+0.000 \pm 0.000$	$+0.000 \pm 0.000$	18.75 ± 0.05
Host	$+0.048 \pm 0.008$	-0.269 ± 0.046	20.28 ± 0.07
HST	$\Delta\alpha\cos\delta('')$	$\Delta\delta('')$	R
QSO A	$+0.000 \pm 0.000$	$+0.000 \pm 0.000$	–
Host	$+0.000 \pm 0.020$	$+0.000 \pm 0.020$	–
Comp.	$+0.400 \pm 0.100$	-1.000 ± 0.100	22.00 ± 0.50
HST	$\Delta\alpha\cos\delta('')$	$\Delta\delta('')$	I_c
QSO A	$+0.000 \pm 0.000$	$+0.000 \pm 0.000$	17.89 ± 0.03
Host	$+0.000 \pm 0.006$	$+0.000 \pm 0.006$	19.70 ± 0.15

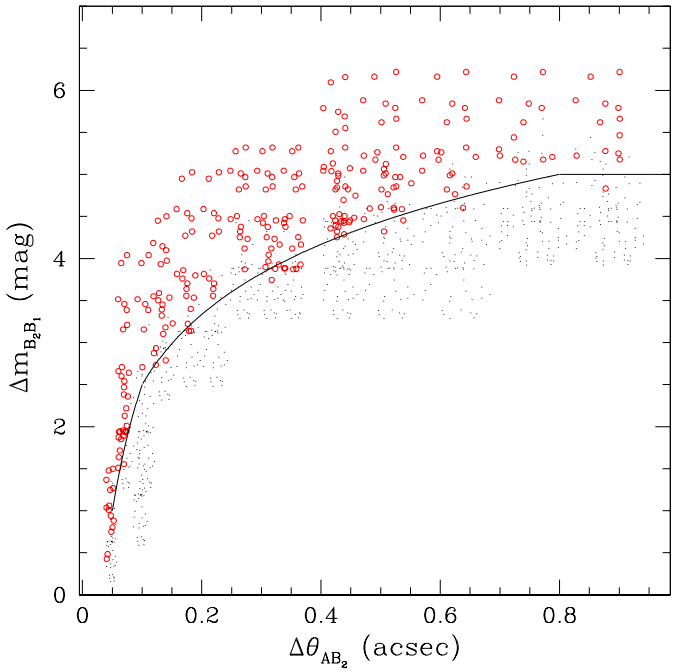

Fig. 3. Angular selection function (ASF) of our HST frames around Q1548+114 A. The ASF curve separates the undetected (circles) from the detected (dots) simulated secondary lensed images B_2 in the vicinity of QSO A.

enough to probe the outermost profile so that its morphological type cannot be found from model fitting. We assume it is an elliptical galaxy since the quasar is radio-loud (e.g. Bahcall et al. 1997).

Finally, our F814W HST images are not saturated and allow for a clean PSF analysis of QSO A, firstly aimed at detecting a faint secondary lensed image B2 of QSO B. As a consequence, the host galaxy appears to be faint and the companion is barely detected so that its photometry cannot be performed. The analysis has been carried out as described in Remy et al. (1998): QSO B has been used to generate an oversampled `TINYTIM` PSF, for the best values of the jitter and focus parameters. As for the NTT frames, simultaneous fits of the PSF together with either a gaussian, exponential or de Vaucouleurs model for the host galaxy have been performed. Is is impossible to indentify which is the best model. The magnitude of QSO A corresponds to the integrated counts number in the scaled PSF while the magnitude of the host galaxy is estimated from the integrated flux in a box of 1 arcsec^2 after a properly scaled PSF subtraction. The errors reported in Table 2 are dominated by the systematic uncertainty on the model. On the other hand, no secondary lensed image of QSO B is seen in the vicinity of QSO A + host galaxy after their subtraction.

3.3. HST detection limit on the secondary lensed image

The empirical determination of the largest magnitude difference between B_2 and $B_1 \equiv B$ detectable with our scaled PSF subtraction technique as a function of the angular separation between B_2 and QSO A (i.e. the angular selection function, ASF) is very important in order to observationally set a realistic constraint on the QSO mass and on the lensing model. To reach this goal, we added to QSO A a synthetic PSF profile generated by `TINYTIM` with shot noise, at random positions and with random intensities. Each resulting image was then analysed in the same way as the original one. The ASF separates the detection and the non detection regions of the plane $\Delta m_{B_2B_1} - \Delta\theta_{AB_2}$ (see Fig. 3). A smoothed fit to the ASF is given by the following relation:

$$\begin{cases} \Delta m_{B_2B_1} = 7.48 + 4.95 \log \Delta\theta_{AB_2} \\ \qquad \text{if } 0.05'' \leq \Delta\theta_{AB_2} \leq 0.1'' \\ \Delta m_{B_2B_1} = 5.27 + 2.77 \log \Delta\theta_{AB_2} \\ \qquad \text{if } 0.1'' \leq \Delta\theta_{AB_2} \leq 0.8'' \\ \Delta m_{B_2B_1} = 5 \\ \qquad \text{if } \Delta\theta_{AB_2} > 0.8'' \end{cases}$$

4. Lens modeling of Q1548+114 A and its environment

We have selected all the observed field galaxies residing within a 45″radius from Q1548+114 A (see Sect. 3.1); the position and the apparent R magnitude estimated by SExtractor for each galaxy are listed in the first columns of Table 3. The corresponding data for the host and the companion galaxy were obtained from the PSF analysis (see Table 2).

All the galaxies, including the companion and the host galaxy of QSO A, are assumed to act as "truncated" Singular Isothermal Spheres (SIS; Katz & Paczyński 1987; Turner et al. 1984). Quasar Q1548+114 A itself is regarded to act as a point mass lens. We also assume that all field galaxies belong to one and same cluster located at z $\sim$ 0.44 which also includes Q1548+114 A and the three galaxies G1-G3 (Stockton 1974). We neglect microlensing by stars in the host galaxy.

The free parameters of our model are the (M/L_R) ratio of the galaxies, the mass M_A of QSO A and the density κ_c of a uniform sheet of dark matter possibly associated with the galaxy cluster.

The individual physical and lensing properties of the field galaxies computed in the frame of the SIS model are listed in the second part of Table 3. Their absolute magnitudes are derived from their apparent R magnitudes with a K-correction of 0.2 mag including evolution (Fioc & Rocca-Volmerange 1997). Assuming that all galaxies are elliptical, we have calculated their corresponding velocity dispersions from their luminosity using the Faber-Jackson relation (Faber & Jackson 1976):

$$\frac{\sigma}{\sigma^*} = \left(\frac{L}{L^*}\right)^{1/4}, \qquad (1)$$

where σ^* is set to 225 km/s and L^* corresponds to $M_R^* = -20.9 + 5 \log h$ ($h = H_o/100$), following the procedure in Fukugita & Turner (1991) and applying a colour term of $b_j - R = 1.54$ (Metcalfe et al. 1991). The value of σ^* is also in agreement with statistical studies of gravitational lensing in highly luminous quasar samples (Claeskens 1999; Kochanek 1996).

Table 3. Observed properties of all objects detected within $45''$ from Q1548+114 A on ground-based observations (see Sect. 3; the properties of the QSO A host galaxy (H) and companion (C) come from the PSF analysis) and computed physical quantities for the field galaxies in the Einstein - de Sitter Universe with $H_o = 65$ km/s/Mpc (see Sect. 4). An M/L_R ratio of 50 has been adopted. "B", "G1", "G2"and "G3" in column "ID" stand for QSO B and galaxies G1-G3 in Fig. 1. The $\Delta\alpha$ and $\Delta\delta$ coordinates are relative to QSO A. Column "Type" refers to a pointlike object (1) or a galaxy (0).

ID#	$\Delta\alpha\cos\delta$ ($''$)	$\Delta\delta$ ($''$)	Type	m_R	M_R	σ (km/s)	θ_E ($''$)	M_{gal} ($M_\odot$)	r_{cut} (kpc)	θ_{cut} ($''$)
30	-7.473	-40.995	0	24.57	-17.36	80.2	.11	2.322E+10	4.9	1.0
36	-26.288	-33.897	0	23.53	-18.40	101.9	.18	6.052E+10	8.0	1.5
39	15.367	-32.768	1	21.78	.00	.0	.00	0.000E+00	.0	.0
40	21.590	-33.364	0	20.09	-21.84	225.1	.87	1.438E+12	38.9	7.5
43	28.660	-28.948	0	25.28	-16.65	68.1	.08	1.207E+10	3.6	.7
44	-21.814	-28.314	0	23.55	-18.38	101.5	.18	5.941E+10	7.9	1.5
46	6.104	-26.876	0	24.05	-17.88	90.4	.14	3.749E+10	6.3	1.2
47	-28.284	-26.794	0	24.30	-17.63	85.4	.13	2.978E+10	5.6	1.1
50	-13.205	-26.182	1	21.47	.00	.0	.00	0.000E+00	.0	.0
51	-17.856	-24.520	0	22.47	-19.46	130.1	.29	1.606E+11	13.0	2.5
57	22.645	-21.221	0	23.28	-18.65	108.0	.20	7.618E+10	8.9	1.7
58	-30.499	-21.139	0	22.07	-19.86	142.7	.35	2.322E+11	15.6	3.0
60	-10.257	-19.380	0	24.04	-17.89	90.6	.14	3.783E+10	6.3	1.2
61	18.631	-18.153	0	24.07	-17.86	90.0	.14	3.680E+10	6.2	1.2
65	23.544	-16.328	0	23.67	-18.26	98.7	.17	5.319E+10	7.5	1.4
68	-4.620	-14.337	0	23.45	-18.48	103.8	.19	6.514E+10	8.3	1.6
69	-13.924	-14.194	0	23.09	-18.84	112.8	.22	9.075E+10	9.8	1.9
70	-27.240	-13.110	0	24.42	-17.51	83.1	.12	2.666E+10	5.3	1.0
72	31.950	-10.994	0	22.83	-19.10	119.8	.25	1.153E+11	11.0	2.1
75	15.310	4.289	0	25.11	-16.82	70.9	.09	1.412E+10	3.9	.7
76	-3.299	-9.967	0	21.93	-20.00	147.4	.37	2.642E+11	16.7	3.2
77	35.546	-7.611	0	24.54	-17.39	80.8	.11	2.387E+10	5.0	1.0
78	3.528	-7.452	0	23.85	-18.08	94.7	.15	4.507E+10	6.9	1.3
79	2.509	-6.119	0	22.87	-19.06	118.7	.24	1.111E+11	10.8	2.1
80	-25.737	-6.324	0	21.66	-20.27	156.8	.42	3.387E+11	18.9	3.6
81	-13.163	-6.414	0	20.87	-21.06	188.1	.61	7.012E+11	27.1	5.2
82	-31.717	-4.943	0	23.79	-18.14	96.0	.16	4.763E+10	7.1	1.4
84	43.782	-4.814	0	22.90	-19.03	117.9	.24	1.081E+11	10.7	2.1
85	-30.348	-4.492	0	23.80	-18.13	95.8	.16	4.719E+10	7.0	1.4
86	38.313	-4.949	0	21.71	-20.22	155.0	.41	3.235E+11	18.4	3.6
89	-23.920	-1.904	1	21.91	.00	.0	.00	0.000E+00	.0	.0
90	16.119	-2.840	0	25.06	-16.87	71.7	.09	1.479E+10	3.9	.8
92	15.397	-2.463	0	23.11	-18.82	112.3	.22	8.910E+10	9.7	1.9
93	-29.215	-2.693	0	22.92	-19.01	117.3	.24	1.061E+11	10.6	2.0
94	13.222	3.471	0	21.61	-20.32	158.6	.43	3.547E+11	19.3	3.7
B 95	4.806	-1.017	1	18.76	.00	.0	.00	0.000E+00	.0	.0
96	-38.396	1.205	0	22.53	-19.40	128.3	.28	1.520E+11	12.6	2.4
G1 97	-8.746	-1.048	0	19.44	-22.49	261.4	1.17	2.617E+12	52.4	10.1
G3 98	-10.772	-3.173	0	19.89	-22.04	235.7	.95	1.729E+12	42.6	8.2
G2 99	-10.948	-.866	0	20.42	-21.51	208.6	.75	1.061E+12	33.4	6.4
H 100	.000	.000	0	20.28	-21.65	215.5	.80	1.207E+12	35.6	6.9
C 101	.400	-1.000	0	22.00	-19.93	145.0	.36	2.477E+11	16.1	3.1
102	-6.671	2.644	0	22.29	-19.64	135.6	.32	1.896E+11	14.1	2.7
103	-21.196	3.032	0	23.57	-18.36	101.0	.18	5.833E+10	7.8	1.5
104	31.512	5.543	0	24.38	-17.55	83.8	.12	2.766E+10	5.4	1.0
105	-43.736	5.017	0	22.98	-18.95	115.7	.23	1.004E+11	10.3	2.0
107	35.517	5.307	1	20.74	.00	.0	.00	0.000E+00	.0	.0
108	7.015	5.953	0	23.01	-18.92	114.9	.23	9.769E+10	10.1	2.0
109	-24.620	7.602	0	24.87	-17.06	74.9	.10	1.761E+10	4.3	.8
110	-11.325	8.068	0	24.78	-17.15	76.4	.10	1.914E+10	4.5	.9
112	25.974	9.352	0	24.01	-17.92	91.3	.14	3.889E+10	6.4	1.2
113	-25.984	9.088	0	23.44	-18.49	104.1	.19	6.575E+10	8.3	1.6

Table 3. (continued)

ID#	$\Delta\alpha\cos\delta$ ($''$)	$\Delta\delta$ ($''$)	Type	m_R	M_R	σ (km/s)	θ_E ($''$)	M_{gal} ($M_\odot$)	r_{cut} (kpc)	θ_{cut} ($''$)
114	-25.271	9.415	0	24.20	-17.73	87.4	.13	3.265E+10	5.9	1.1
115	-13.839	10.175	0	23.31	-18.62	107.2	.20	7.411E+10	8.8	1.7
116	-6.826	10.222	1	22.68	.00	.0	.00	0.000E+00	.0	.0
117	-31.054	10.884	0	22.65	-19.28	124.8	.27	1.361E+11	12.0	2.3
120	38.698	11.837	0	24.98	-16.95	73.0	.09	1.592E+10	4.1	.8
122	3.031	12.063	0	24.41	-17.52	83.2	.12	2.691E+10	5.3	1.0
123	35.130	12.734	0	22.62	-19.31	125.7	.27	1.399E+11	12.1	2.3
124	.537	12.565	1	22.07	.00	.0	.00	0.000E+00	.0	.0
128	27.709	13.982	0	20.66	-21.27	197.4	.67	8.509E+11	29.9	5.8
129	20.446	15.896	0	21.80	-20.13	151.8	.40	2.978E+11	17.7	3.4
130	4.963	16.848	0	23.73	-18.20	97.4	.16	5.033E+10	7.3	1.4
131	-33.081	18.466	0	22.92	-19.01	117.3	.24	1.061E+11	10.6	2.0
132	-3.764	19.784	0	23.47	-18.46	103.4	.18	6.395E+10	8.2	1.6
135	16.476	23.323	0	23.38	-18.55	105.5	.19	6.948E+10	8.5	1.6
136	-37.215	24.236	0	24.36	-17.57	84.2	.12	2.818E+10	5.4	1.1
137	-3.748	24.670	0	24.85	-17.08	75.2	.10	1.794E+10	4.3	.8
138	-12.296	25.729	0	23.27	-18.66	108.2	.20	7.689E+10	9.0	1.7
139	-12.502	26.383	0	25.47	-16.46	65.2	.07	1.014E+10	3.3	.6
140	-12.218	26.669	0	25.81	-16.12	60.3	.06	7.411E+09	2.8	.5
142	-13.559	27.323	0	22.68	-19.25	124.0	.26	1.324E+11	11.8	2.3
144	-24.332	29.426	0	22.16	-19.77	139.8	.34	2.137E+11	15.0	2.9
145	-28.307	28.477	0	20.26	-21.67	216.5	.80	1.230E+12	35.9	6.9
147	32.871	29.810	0	20.54	-21.39	202.9	.71	9.503E+11	31.6	6.1
148	29.660	31.958	0	23.34	-18.59	106.5	.19	7.209E+10	8.7	1.7
149	12.744	33.742	0	23.40	-18.53	105.0	.19	6.821E+10	8.5	1.6
150	-7.702	33.911	0	22.83	-19.10	119.8	.25	1.153E+11	11.0	2.1
151	-28.558	33.864	1	21.63	.00	.0	.00	0.000E+00	.0	.0
152	-.239	35.339	0	22.08	-19.85	142.4	.35	2.301E+11	15.5	3.0
155	-18.118	37.734	0	24.42	-17.51	83.1	.12	2.666E+10	5.3	1.0
156	-21.306	37.572	0	25.78	-16.15	60.7	.06	7.618E+09	2.8	.5
157	-21.527	37.882	0	25.06	-16.87	71.7	.09	1.479E+10	3.9	.8

The angular Einstein radius θ_E is then derived according to the well known formula for SIS (e.g. Schneider et al. 1992):

$$\theta_E = \frac{4\pi\sigma^2}{c^2}\frac{D_{DS}}{D_{OS}}\,, \tag{2}$$

where D_{DS} and D_{OS} are the cosmological angular distances between the deflector and the source and the observer and the source, respectively. Let us note here that, whatever the cosmological model, the angular Einstein radius of the QSO A host galaxy is always smaller than half the angular distance between QSO A and QSO B ($2.45''$). Thus, we would never expect a secondary lensed image B_2 to be produced by the host alone (e.g. Refsdal & Surdej 1994).

The SIS model actually describes the halo of the galaxies. Its surface mass density is truncated at r_{cut} such that the SIS deflection angle is equal to that of the Schwarzschild lens with mass M_{gal}:

$$r_{cut} = \frac{G\,M_{gal}}{\pi\,\sigma^2}\,. \tag{3}$$

The mass of the galaxies M_{gal} is computed from their luminosity for a given mass-to-light ratio (M/L_R) expressed in solar units, and adopting for the Sun the absolute magnitude $M_{R,\odot} = 4.31$ (Allen 1976). Thus, changing the (M/L_R) ratio does only affect the cut-off radius, and not the Einstein radius of the lens. The galactic masses listed in Table 3 correspond to $(M/L_R) = 50$. Fig. 4 illustrates the angular cut-off radius and position of the galaxies in the lens plane. The angular cut-off radius of the quasar A host galaxy amounts to $7''$, equivalent to 36 Kpc in the lens plane[2]. Note that the *angular* cut-off radius is independent of Ω_o and λ_o.

Now, how to compute the secondary lensed image properties? For a given mass distribution in the lens plane, the true position of the source (Q1548+114 B) is derived from the observed primary image position (B_1). Then, the flux ratio between the primary image (B_1) and a possible secondary lensed image (B_2) of Q1548+114 B is computed by means of the ray shooting method (Schneider et al. 1992), which includes the shear effect of all field galaxies. In order to simulate the possible formation of image B_2, we chose a very small circular source

[2] In the SIS model, the radius of the spherical halo containing the equivalent mass M_{gal} is given by $R_H = \pi/2 r_{cut}$ and thus would extend up to 56 Kpc for the host galaxy.

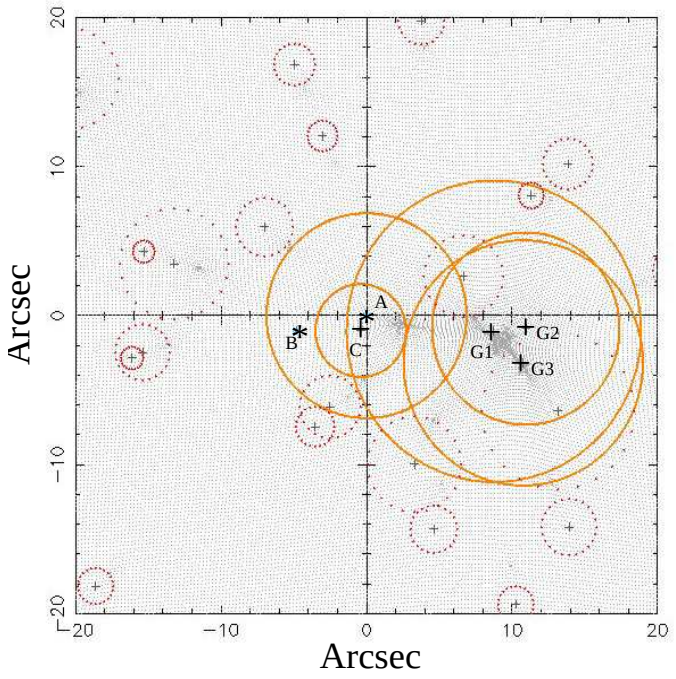

Fig. 4. Circles with angular cut-off radii of SIS models associated with each galaxy in the vicinity of Q1548+114 A ($M/L_R = 50$). Continuous (resp. dotted) circles correspond to galaxies with known (resp. unknown) redshifts. The two asterisks indicate the positions of Q1548+114 A & B and the crosses the center positions of field galaxies. The background shows the caustic network. North is up and East to the left.

($\theta_s \sim 5\,10^{-9''}$)[3], which corresponds to a QSO continuum emitting region of $\sim 10^{14}$ cm. In the ray shooting calculations, we have finally used a very fine grid whose size is one thousandth the diameter of the source, so that within a square surrounding the unlensed source, 10^6 rays are being shot. The results for the expected magnitude difference between the B_1 and B_2 lensed images are presented and discussed in the next section.

5. Upper limits on the mass of quasar Q1548+114 A

5.1. Results

No secondary lensed image B_2 has been detected in the close vicinity of QSO A. For each lens model, the expected flux ratio of the lensed images $I(B_2)/I(B_1)$ can be displayed as a function of the angular separation between B_2 and QSO A. These curves being parametrized as a function of the mass M_A of QSO A, their intersections with the HST ASF derived in Sect. 3.3 yield the corresponding upper limits on M_A. Results for different lens models are presented in Fig. 5 and in Table 4.

A qualitative analysis of Fig. 5 first shows that all curves are very close to each other. A secondary lensed image could therefore not be detected closer than $\sim 0.55''$ from QSO A because it would be too faint. This quasi-degeneracy is due to at least three reasons: i) a secondary image can only be produced by the point mass associated with QSO A since $\theta_{E,Host} = 0.8''$ is smaller than half the angular distance between images A and B; ii) for small angular separations, the shear effect of the point mass dominates, so that all curves merge at very small angular separations ($\Delta\theta \to 0$); iii) the effect of the three bright galaxies is weaker than in Iovino & Shaver (1986), as we replaced for these the (unrealistic) point mass model with the SIS model: increasing the mass of the galaxies results in expanding their halo instead of deepening their gravitational well.

[3] The exact source size is not important as the source lies far from any caustic (see Fig. 4).

Table 4. Mass constraints (in $M_\odot$) on QSO A for the lensing model with point mass + host + companion + G1-G3.

	$M/L_R = 10$	$M/L_R = 50$
$\kappa_c = 0$	$4.7\,10^{11}$	$4.4\,10^{11}$
$\kappa_c = 0.2$	$3.6\,10^{11}$	$3.3\,10^{11}$

However, the mass parametrization is not the same on the different curves. The host galaxy as well as the new close companion help in producing a secondary image, while galaxies G1-G3 counteract the influence of QSO A. The latter effect is best seen on the $M/L_R = 50$ curves (see Fig. 5A) since the angular cut-off radii of G1 and G3 then extend up to QSO A. However, the exact value of M/L_R has little influence on the final results (see Table 4). On the other hand, the overall tidal shear ($\gamma = 0.012$) produced by the remaining 70 field galaxies has a negligible effect on the results (see the large crosses in Fig. 5A). Simulations show that this remains true if we assume that the field galaxies are not at the redshift of QSO A. Thus, the corresponding external shear can be neglected.

Finally, assuming that all field galaxies belong to one and same cluster at $z = 0.44$, the associated surface mass density κ_c is about 0.025 in units of the critical density for $M/L_R = 30$ ($\Sigma_{\rm crit} \simeq 0.5$ g/cm^2). If we consider that 90% of the mass of the cluster is dark matter, we find that the latter acts as a uniform sheet of matter with a maximum surface density $\kappa_c = 0.2$. The mass constraint is then stronger since the cluster contributes to the image angular separation (see Fig. 5B and Table 4).

The limits on M_A presented in Table 4 scale as H_o^{-1}. Choosing a flat cosmology dominated by the cosmological constant reinforces the constraints on M_A by only $\sim 25\%$ so that our results are robust and conservative with respect to the exact values of the cosmological parameters.

5.2. Discussion

Due to the modeling of galaxies by means of SIS, the constraint on the mass of QSO A ($M_A < 4.5\,10^{11}{\rm M}_\odot$) is little sensitive to the adopted values of the model parameters. This new upper limit is only 4 times smaller than the value proposed by Iovino & Shaver (1986) but it is a robust estimate built on observed galaxy magnitudes and on a realistic ASF. How does this limit compare with other estimations? First, computing the QSO A bolometric luminosity from the R luminosity using $L_{\rm bol} \simeq 43 L_R$ (as derived from Fig. 7 in Laor & Draine 1993) and L_R being computed from the apparent magnitude of

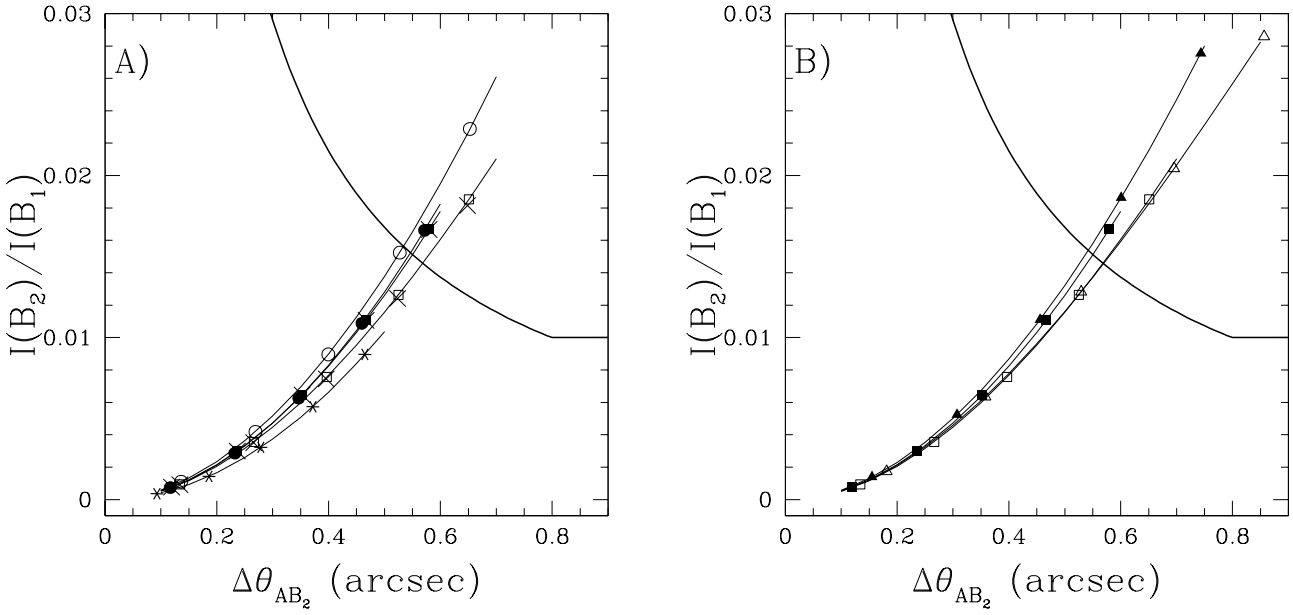

Fig. 5a and b. Intensity ratio between the lensed images ($B_1 \equiv B$ and B_2) as a function of the angular separation between B_2 and Q1548+114 A for different lensing models. The same symbols represent a QSO A mass of 1, 2, 3, 4 and 5 in units of $10^{11}\mathrm{M}_\odot$; filled symbols for $M/L_R = 10$ and open symbols for $M/L_R = 50$. A) point mass (*), point mass + host (circles), point mass + host + companion + G1-G3 (squares); the large crosses indicate the result when considering the (very small) influence of all the other field galaxies. B) point mass + host + companion + G1-G3 with $\kappa_c = 0$ (squares) and $\kappa_c = 0.2$ (triangles). On both graphs, the thick line represents the observed ASF.

QSO A in Table 2, the minimum Eddington mass of the MBH is found to be approximately $1.5\,10^8\mathrm{M}_\odot$. On the other hand, Laor (1998) presents a correlation between the MBH mass and the absolute V magnitude of the host, based on BLR measurements and HST host observations. Adopting $V - R \sim 1$ (Fukugita et al. 1995) for the host, we get $M_{\mathrm{MBH}} \simeq 2\,10^8\mathrm{M}_\odot$. Finally, the correlation between the mass of the bulge and the mass of the MBH proposed by Magorrian et al. (1998) for local normal galaxies would yield with our measurement of the host absolute magnitude $M_{\mathrm{MBH}} \simeq 10^9\mathrm{M}_\odot$ for $M/L_R = 10$.

Our upper limit on M_A thus remains more than two orders of magnitude above current estimates. On the other hand, our non-detection of a secondary lensed image is fully compatible with the expected mass of QSO A. If this secondary image was unseen because of extinction by dust, the resulting value of M_A would then be in conflict with the other estimates.

6. HST direct imagery of Q1148+0055 A & B

Q1148+0055 A & B ($z_A = 1.89$, $z_B = 1.41$, $\Delta\theta = 3.9''$) has been identified in a search for new gravitational lens systems within a sample of highly luminous quasars (Surdej et al. 1993; see also Hewett et al. 1994). The angular separation between these two quasars turns out to be the smallest one presently known among pairs with different redshifts. The published V magnitudes of the two objects are $V_A = 18.2$ and $V_B = 21.2$ (Hewett et al. 1998). Thus, the most distant QSO being also the brightest, the detection of a secondary image should be easier.

Q1148+0055 A & B have been imaged in April 1999 with the WFPC2 planetary camera onboard HST through the F555W filter (4×400 sec), and through the F814W filter (2×1300 sec) to search for closeby galaxies (PID 6790). The photometry in F555W and the relative astrometry of Q1148+0055 A & B have been performed using a PSF subtraction as described in Sect. 3.2; they are reported in Table 5. QSO B is found to lie at $3.883'' \pm 0.001''$ and P.A.$= 111.05^\circ \pm 0.05$ from QSO A, confirming the values of $3.9'' \pm 0.1''$ and $111^\circ \pm 2^\circ$ derived by Hewett et al. (1998). No secondary lensed image of QSO A is detected in the close angular vicinity of QSO B. The images of the QSOs are saturated on the F814W frames but the galaxy detected in infrared by Hewett et al. (1998) is clearly seen at $\Delta\theta = 5.24'' \pm 0.05''$ and P.A.$= 274.9^\circ \pm 0.1^\circ$. Its magnitude within a circle of $1''$ radius is $I_c = 21.4 \pm 0.1$. From the K magnitude published by Hewett et al. (1998), we find $I_c - K = 3 \pm 0.25$. This could be the colour of a $\sim 0.3L_*$ elliptical galaxy located at $z \sim 0.6 - 0.8$ (Fioc & Rocca-Volmerange 1997; Songaila et al. 1994).

We estimated the ASF as described is Sect. 3.3. Without any clues on the host of Q1148+0055 B, the lensing model is simply reduced to a single point mass for Q1148+0055 B and one truncated SIS for the closeby galaxy. Ray shooting simulations show that the absence of a secondary lensed image

Table 5. Photometry in the F555W≃V filter and relative astrometry for Q1148+0055 A & B.

	$\Delta\alpha\cos\delta('')$	$\Delta\delta('')$	V
QSO A	$+0.000 \pm 0.000$	$+0.000 \pm 0.000$	18.00 ± 0.01
QSO B	$+3.623 \pm 0.001$	-1.396 ± 0.001	21.60 ± 0.05

A_2 with a flux larger than 0.1% the flux of Q1148+0055 A and located further away than $0.25''$ from Q1148+0055 B implies that the combined mass of the latter and its host must be smaller than $6.5\,10^{11}\mathrm{M}_\odot$. This results is very little dependent on the adopted M/L_R for the galaxy.

7. Conclusions

On the basis of new HST direct images, we constrained the mass of Q1548+114 A and Q1148+0055 B from the non detection of secondary lensed images of the background quasars located very close to the lines-of-sight. All the detected field galaxies have been taken into account in the ray shooting simulations, including the host when visible. The derived maximal mass of Q1148+0055 B plus its host has been estimated to $6.5\,10^{11}\mathrm{M}_\odot$ while that of the central pointlike component of Q1548+114 A is $4.5\,10^{11}\mathrm{M}_\odot$. These limits are robust with respect to the adopted M/L_R ratio and redshift for the field galaxies and to the exact values of Ω_o and λ_o. They scale as H_o^{-1}.

The upper limit on the central mass of Q1548+114 A is in full agreement with independent estimates of $\sim\ 10^9\mathrm{M}_\odot$. As the latter are based on several assumptions, gravitational lensing provides a valuable check. This is also an important argument to say that extinction should not be critical in our observations. Unfortunately, improving the sensitivity of this technique within the expected QSO mass range requires unrealistically high angular resolution and dynamic (see Fig. 5). The discovery of a distant quasar very close to the line-of-sight of a local one ($z \leq 0.1$) would help in strenghtening the mass constraint, provided the host galaxy of the latter does not spoil the detection of the secondary lensed images.

In the course of our study, we performed photometry and relative astrometry of all objects detected in the QSO fields, using PSF fitting to analyse the close angular vicinity of the quasars. The host and the presence of a close companion of Q1548+114 A have been reported.

Acknowledgements. This research was supported in part by contract P4/05 "Pôle d'Attraction Interuniversitaire" (OSTC, Belgium), by the "Fonds National de la Recherche Scientifique" (Belgium) and by PRODEX (Gravitational lensing studies with HST).

References

Allen C.W., 1976, Astrophysical Quantities. 3^{rd} edition, 162p
Bahcall J.N., Kirkhakos S., Saxe D.H., Schneider D.P., 1997, ApJ 479, 642
Barthel P.D., Miley G.K., Schilizzi R.T., Preuss E., 1984, A&A 140, 399
Bertin E., Arnouts S., 1996, A&AS 117, 393
Burki G., Rufener F., Burnet M., et al., 1995, A&AS 112, 383, http://archive.eso.org/wdb/wdb/eso/extinctions/form
Claeskens J.-F., 1999, Thèse de Doctorat, Soc. Roy. Sci. Liège 68 1-4, pp. 1-305
Faber S.M., Jackson R.E, 1976, ApJ 204, 668
Fioc M., Rocca-Volmerange B., 1997, A&A 326, 950
Fukugita M., Turner E.L., 1991, MNRAS 253, 99
Fukugita M., Shimasaku K., Ichikawa T., 1995, PASP 107, 945
Gott J.R., Gunn J.E., 1974, ApJ 190, L105
Hewett P.C., Irwin M.J., Foltz C.B., et al., 1994, AJ 108, 1534
Hewett P.C., Foltz C.B., Harding M.E., Lewis G.F., 1998, AJ 115, 383
Holtzman J.A., Burrows C.J., Casertano S., et al., 1995, PASP 107, 1065
Iovino A., Shaver P., 1986, A&A 166, 119
Katz N., Paczynski B., 1987, ApJ 317, 11
Kochanek C.S., 1996, ApJ 466, 638
Krist J., Hook R., 1996, http://scivax.stsci.edu/∼krist/tinytim.html
Krolik J.H., 1999, Active Galactic Nuclei. Princeton University Press
Landolt A.U., 1992, AJ 104, 340
Laor A., 1998, ApJ 503, L83
Laor A., Draine B.T., 1993, ApJ 402, 441
Magorrian J., Tremaine S., Richstone D., 1998, AJ 115, 2285
Metcalfe N., Shanks T., Fong R., Jones L.R., 1991, MNRAS 249, 498
Padovani P., Rafanelli P., 1988, A&A 205, 53
Refsdal S., Surdej J., 1994, Rep. Prog. Phy. 56, 117
Remy M., 1997, Thèse de Doctorat, Université de Liège
Remy M., Claeskens J.-F., Surdej J., et al., 1998, New Astr. 3, 379
Shaver P., Robertson J.G., 1985, MNRAS 212, 15p
Schneider P., Ehlers J., Falco E.E., 1992, In: Harwitt M., Kippenhahn R., Trimble V., Zahn J.-P. (eds.) Gravitational lenses. A&A Library, Springer-Verlag
Songaila A., Cowie L.L., Hu E.M., Gardner J.P., 1994, ApJS 94, 461
Stockton A., 1974, Nat 250, 308
Stockton A., MacKenty J.W., 1987, ApJ 316, 584
Surdej J., Remy M., Smette A., et al., 1993, In: Surdej J., Fraipont-Caro D., Gosset E., et al. (eds.) Proc. of the 31st Liège International Astrophysical Colloquium, p. 153
Surdej J., et al., 2000, in preparation
Turner E.L., Ostriker J.P., Gott J.R., 1984, ApJ 284, 1
Wampler E.J., Baldwin J.A., Burke W.L., et al., 1973, Nat 246, 203
Whitmore B., 1997, http://www.stsci.edu/ftp/instrument_news/WFPC2/Wfpc2_phot/photom2.ps
Yee H.K.C., Green R.F., Stockman H.S., 1986, ApJS 62, 681